Centrosome Loss And Cell Proliferation Defects Underlie Developmental Failure In Haploid Zebrafish Larvae

Kan Yaguchi[1,2], Daiki Saito[1], Triveni Menon[3], Akira Matsura[1], Takeomi Mizutani[4], Tomoya Kotani[5], Sreelaja Nair[6], and Ryota Uehara[1,2]

[1]Graduate School of Life Science, Hokkaido University, Kita 21, Nishi 11, Kita-Ku, Sapporo, 001-0021, Japan
[2]Faculty of Advanced Life Science, Hokkaido University, Kita 21, Nishi 11, Kita-Ku, Sapporo, 001-0021, Japan
[3]Department of Molecular Biology, Princeton University, New Jersey 08544, USA
[4]Department of Life Science and Technology, Faculty of Engineering, Hokkai-Gakuen University, Minami 26, Nishi 11, Chuo-ku, Sapporo, 064-0926, Japan
[5]Department of Biological Sciences, Faculty of Science, Hokkaido University, Kita 10, Nishi 8, Kita-Ku, Sapporo 060-0810, Japan
[6]Department of Biosciences and Bioengineering, Indian Institute of Technology Bombay, Powai, Mumbai, 400076, India

Corresponding authors:

Sreelaja Nair, Department of Biosciences and Bioengineering, Indian Institute of Technology Bombay, Powai, Mumbai, 400076, India
E-mail: sreelaja@iitb.ac.in
Phone: 91-22-25766758

Ryota Uehara, Faculty of Advanced Life Science, Hokkaido University, Kita 21, Nishi 11, Kita-Ku, Sapporo 001-0021, Japan
E-mail: ruehara@sci.hokudai.ac.jp
Phone: 81-11-706-9238

Preprint Servers: BioRxiv

Classification: Biological Sciences, Developmental Biology

Keywords: Ploidy, Centrosome, Zebrafish

Abstract

Haploid embryonic lethality is a common feature in vertebrates. However, the developmental defects and timing of lethality in haploid embryos differ between non-mammalian and mammalian species. Therefore, it remains unknown whether vertebrates share common principles of haploid intolerance. We investigated haploidy-linked defects at the cellular level in gynogenetic haploid zebrafish larvae that manifest characteristic morphogenetic abnormalities. Haploid larvae suffered severe mitotic arrest and irregular upregulation of p53, leading to unscheduled cell death. Either mitigation of mitotic arrest by spindle assembly checkpoint inactivation or depletion of p53 significantly improved organ growth in haploid larvae, indicating the critical contribution of these cellular defects to haploidy-linked morphogenetic defects. Moreover, haploid zebrafish larvae suffered frequent centrosome loss resulting in mitotic spindle monopolarization, a leading cause of mitotic instability in haploid mammalian cells (1, 2). Haploid larvae also suffered ciliopathy associated with severe centrosome loss. Based on our results, we propose the ploidy-linked alteration in centrosome number control as a common principle constraining the allowable ploidy state for normal development in vertebrates.

Significance statement

Haploid embryos possessing a single chromosome set are invariably lethal in vertebrates. Though haploid intolerance is attributed to imprinting misregulation in mammals, it remains unknown what limits the developmental capacity of haploid non-mammalian vertebrates free from the imprinting constraint. This study revealed the haploidy-linked mitotic misregulation and p53 upregulation as the leading cause of organ growth retardation in haploid zebrafish larvae. Accompanied by these defects, haploid larvae manifested drastic centrosome loss and mitotic spindle monopolarization, defects also limiting the proliferative capacity of haploid mammalian cells. These findings suggest the ploidy-linked alteration in centrosome number control as a common cell-intrinsic principle of haploid intolerance in vertebrates, providing an insight into an evolutionary constraint on allowable ploidy status in animal life cycles.

Introduction

Eukaryotic life cycles have evident diversity with flexibility in ploidy states of the somatic growth phase. For example, plants and fungi have both haplontic and diplontic life cycles, where multicellular development occurs in the haploid and diploid states, respectively (3). In animals, although some orders of invertebrates have haplodiplontic life cycles, all vertebrates are diplontic (3, 4). Haploid embryos generated through egg activation without the contribution of one parent's genome (e.g., parthenogenesis, gynogenesis, or androgenesis) are almost invariably lethal in vertebrates, showing that diploidy is required to complete embryonic development in the sub-phylum (5). In mammals, haploid embryonic lethality is mainly attributed to the misregulation of imprinted genes. Differential expression of parental alleles of imprinted genes disables the development of mammalian uniparental haploid embryos beyond implantation (6, 7). Additionally, mammalian haploid embryos suffer chromosomal instability and ploidy alterations due to chromosome missegregations even during pre-implantation stages (8-10).

On the other hand, non-mammalian vertebrates are devoid of parent-specific genomic imprinting and hence free from imprinting-associated developmental defects. Moreover, fish or amphibian haploid embryos develop until the late larval stages without drastic changes in the ploidy state, indicating that haploidy is stable in these species compared to mammals (11-14). However, despite the lack of the detrimental features of imprinting misregulation and

haploid instability, non-mammalian vertebrate haploid embryos manifest severe morphological defects with poor growth of organs such as the brain and eyes and succumb to lethality after hatching (12, 14-18). Forced diploidization of these haploid embryos by artificial induction of whole-genome duplication in the early cleavage stages resolves these developmental defects, suggesting that the haploid state per se, rather than loss of heterozygosity of deleterious recessive alleles, causes these defects (13, 19-21). Therefore, understanding how ploidy influences specific processes during organogenesis will provide fundamental insights into the relevance of the diploid state in vertebrate somatic development.

Non-mammalian vertebrates provide opportunities for investigating the influence of haploidy on organogenesis. For example, studies in fish or amphibians have revealed haploidy-linked defects in collective cell migration during gastrulation (22), water inflow control through ectoderm in gastrulae (23), and morphology and spatial arrangements of cells in the embryonic epidermis during post-gastrula stages (24, 25). However, the direct cause of poor organ growth in haploid embryos remains unknown, particularly at the level of intrinsic cellular control. Moreover, it remains undetermined whether non-mammalian and mammalian vertebrates share common principles of haploidy intolerance.

In this study, we investigated cellular defects in haploid zebrafish during the larval stages, when organ growth abnormality becomes evident (26). We found a drastic increase in unscheduled cell death associated with severe mitotic arrest and p53 upregulation in haploid

larvae. Mitigation of mitotic arrest or p53 upregulation significantly improved organ growth, indicating that haploidy-linked poor organ growth stems mainly from these cellular defects. Moreover, haploid zebrafish larvae suffered frequent centrosome loss resulting in monopolar mitotic spindles, a feature also observed in mammalian cells (1). Based on our results, we propose the ploidy-linked alteration in centrosome number control as a common cellular principle that constrains the allowable ploidy state for normal development in vertebrate organisms.

Results

A drastic increase in unscheduled apoptosis in haploid larvae

We investigated the developmental processes of haploid and diploid zebrafish larvae generated by *in vitro* fertilization using UV-irradiated and non-irradiated spermatozoa, respectively (Fig. S1). At 3.5 days post fertilization (dpf), by which most organs formed, haploid larvae manifested typical "haploid syndrome" defects, such as curled, short body axis and reduced brain and eye sizes compared with diploid counterparts (Fig. 1A and B) (14, 18, 26, 27). The morphological defects of haploid syndrome occurred in varying phenotypic grades, with some larvae manifesting severe defects and others with milder defects within a clutch (Fig. 1A). Consistent with this, we observed a larger range in body and organ size distributions in haploid larval groups than in diploids (Fig. 1B). DNA content analysis using flow cytometry showed that the 1C and 2C populations (possessing one and two genome copies, respectively) predominated in the haploid larval groups at 3 and 5 dpf, confirming that haploid zebrafish larval cells retained the haploid state throughout the time duration (Fig. S1). This is in sharp contrast to haploid mammalian embryonic cells that quickly convert to diploids during early embryogenesis (9, 10).

To gain insights into haploidy-linked developmental defects at the cellular level, we investigated cell viability in 3 dpf haploid and diploid larvae by visualizing apoptosis using whole-mount immunostaining of active caspase-3. In diploid larvae, active caspase-3-positive cells were infrequent and found at specific sites, such as the optic tectum, mid-brain,

and the inner retinal layers (Fig. 2A, B, and S2), presumably reflecting programmed apoptosis underlying tissue organization (28). On the other hand, in haploid larvae, active caspase-3 positive cells were frequently detected throughout the whole body (Fig. 2A, B, and S2). We also observed clusters of apoptotic cells in the retinal periphery and brain ventricles in haploid larvae (Fig. 2A and S2, see also Fig. 2B). These results demonstrate that haploid larvae suffer unscheduled apoptosis throughout the body, potentially impairing organ growth and patterning during development.

Irregular p53 upregulation limits organ growth in haploid larvae

Since unscheduled apoptosis may underlie the developmental defects in haploid larvae, we next sought to determine the cause of the haploidy-linked unscheduled apoptosis. As a candidate apoptosis inducer, we investigated expression levels of p53 protein in haploid and diploid larvae at 3 dpf by immunoblotting (Fig. 3A). We found that the expression of full-length p53 was significantly higher in haploid larvae than in diploids (Fig. 3A and B). p53 level in haploids was even higher than that in diploid larvae irradiated with UV, in which DNA damage-associated upregulation of p53 occurred (Fig. 3B).

To gain insights into the causality between unscheduled p53 upregulation and haploidy-linked defects, we suppressed p53 expression using a morpholino and tested its effects on cell viability in haploid larvae by detecting caspase-3-positive cells by immunostaining. p53-targeting morpholino substantially reduced the expression of both p53 full-length and shorter

isoforms (Fig. 3C and D). Immunostaining revealed that cleaved caspase-3-positive cells were less frequently observed in haploid p53 morphants than in control haploid larvae injected with a 4-base mismatch morpholino or uninjected haploid larvae (Fig. 3E, F, and S3A; see also Fig. 2). We also found that apoptotic cell clusters frequently observed in haploid larvae were absent in haploid p53 morphants (Fig. 3F and S3A). DNA content in haploid p53 morphants was equivalent to that in control haploids, demonstrating that the ploidy level did not change upon p53 suppression in haploid larvae (Fig. S3B). These results suggest that increased levels of p53 significantly contribute to enhanced apoptosis in haploid larvae.

We also tested the effect of p53 suppression on organ growth in haploid larvae (Fig. 3G). Suppression of p53 expression significantly increased body-axis length and brain width assessed at the mid-brain in haploid larvae (Fig. 3G and H). Analysis of organ size distribution also revealed that p53 suppression notably eliminated the population of haploid larvae that suffered particularly severe organ size reduction, suggesting efficient alleviation of the haploidy-linked poor organ growth (Fig. 3H). The above data indicate p53-induced apoptosis as a primary cause of haploidy-linked organ growth retardation.

Haploidy-linked mitotic arrest compromises cell proliferation leading to organ growth defects in haploid larvae

176 The finding of p53 upregulation in haploid larvae prompted us to further investigate
177 haploidy-specific defects in cell proliferation. We conducted flow cytometry of haploid and
178 diploid whole-larval cells stained with Hoechst and fluorescence-conjugated anti-phospho-
179 histone H3 (pH3) antibody to mark DNA and mitotic chromosomes, respectively, at 1-3 dpf
180 (Fig. 4A and B). In diploid larvae, the proportion of pH3-positive mitotic cells was 1.6 % at
181 1 dpf, which decreased to 0.4% at 3 dpf (Fig. 4A and B), likely reflecting the transition from
182 proliferative to postmitotic state in different cell lineages during larval stages (29, 30). On
183 the other hand, the proportion of pH3-positive cells in haploid larvae was 1.6% at 1 dpf and
184 remained 1.2% at 3 dpf (Fig. 4A and B). The mitotic index was significantly higher in haploid
185 larvae than in diploids at 2-3 dpf (Fig. 4B). Additionally, whole-mount immunostaining
186 showed an increase in pH3-positive cells in haploids at 3 dpf compared to diploids (Fig. 2A).

187

188 The increased mitotic index seen in 2-3 dpf haploid larvae could arise from defects in the
189 temporal control of postmitotic transition in different tissues. Alternatively, delay or arrest in
190 the progression of each mitotic event could also cause a net increase in the mitotic population.
191 To specify the cause of the abnormal increase in the mitotic index in haploid larvae, we
192 conducted live imaging and analyzed the mitotic progression of endothelial cells in 1.5-3 dpf
193 haploid and diploid larvae stably expressing histone-H2B-mCherry (Tg(fli1:h2b-
194 mCherry)/ncv31Tg) (31). In diploid larvae, almost all cells that entered mitosis (marked by
195 nuclear envelope break down (NEBD)) completed chromosome alignment and segregation
196 within 30 min after mitotic entry (Fig. 4C and D). On the other hand, 15% of haploid cells

197 spent > 60 minutes in the mitotic phase, revealing a severe mitotic delay in haploid larvae.
198 Such mitotically delayed haploid cells often underwent mitotic death or mitotic slippage
199 (exiting mitosis without proper chromosome segregation) (Fig. 4C and E). Mitotic
200 progression was slower in haploid larvae than in diploids for the duration of assessment from
201 1.5-3 dpf, with more frequent mitotic defects later in the observation (Fig. S4A, B, and D).
202 We also observed severe chromosome misalignment in haploid cells delayed in mitosis (Fig.
203 4C), suggesting that the increased mitotic index and mitotic delay seen in haploid larvae
204 could be due to the activation of the spindle assembly checkpoint (SAC).

205

206 Next, we sought to resolve the haploidy-linked mitotic arrest by suppressing SAC using
207 reversine, an inhibitor of Mps1 kinase required for SAC activation (32). In live imaging of
208 histone-H2B-mCherry, 97% of reversine-treated haploid larval cells underwent chromosome
209 segregation or exited mitosis within 30 min after NEBD (Fig. 5A, B, and S4C). Notably, cells
210 in reversine-treated haploid larvae underwent mitotic death less frequently than those in non-
211 treated haploids (Fig. 5C, see also Fig. 4E). Therefore, SAC inactivation resolved the severe
212 mitotic delay and partially mitigated mitotic cell death in haploid larvae.

213

214 If the abnormal cell proliferation in haploid larvae indicated by the high mitotic index was
215 due to mitotic delay from SAC activation, SAC inactivation could resolve it. We tested the
216 effect of reversine treatment on the mitotic index in 3 dpf haploid larvae using flow cytometry
217 (Fig. 5D and E). Reversine treatment significantly reduced the proportion of pH3-positive

218 cells in haploid larvae to levels equivalent to that in diploids (Fig. 5D and E, see also Fig. 4A
219 and B). In immunostained haploid larvae, we also observed a reduction in pH3-positive cells
220 across tissues upon reversine treatment (Fig. 5F). These results indicate that the abnormally
221 high mitotic index is mainly due to the SAC-dependent mitotic arrest rather than defects in
222 the developmental program of cell division control.

223

224 Based on the finding that SAC inactivation mitigated the abnormal cell proliferation in
225 haploid larvae, we next tested the effect of reversine treatment on organ growth in haploid
226 larvae. Reversine treatment significantly increased body axis length and eye size in haploid
227 larvae compared to DMSO-treated control (Fig. 5G and H). These results indicate that the
228 haploidy-linked mitotic stress with SAC activation is a primary constraint for organ growth
229 in haploid larvae.

230

231 **Haploidy-linked centriole loss underlies mitotic defects in haploid larvae**

232 To understand the cause of SAC activation in haploid larvae, we next investigated mitotic
233 spindle organization by immunostaining of centrin and α-tubulin, which mark the centrioles
234 and microtubules, respectively, in the eyes, brain, and surface epithelia in the head region of
235 haploid and diploid larvae from 0.5 to 3 dpf (Fig. 6 and S5). In diploids, almost all mitotic
236 cells possessed bipolar spindle with the normal number of 4 centrioles in all stages tested. At
237 0.5 dpf, haploid embryonic cells also possessed bipolar spindle with 4 centrioles (Fig. 6A-C,
238 and S5A-C). However, as development progressed, cells in haploid larvae had monopolar

239 spindles with reduced centriole number and severe chromosome misalignment. In the eyes,
240 brain, skin, and olfactory organ of haploid larvae, 14.5% of mitotic cells had monopolar
241 spindles at 1 dpf, which increased to 32.9% and 61.5% at 2 and 3 dpf, respectively (Fig. 6B).
242 This increase in the cell population with monopolar spindles corresponded well with the
243 stage-dependent increase in mitotic cells with reduced centriole number (Fig. 6C). The
244 trajectory of centriole loss was organ-specific: centriole loss and spindle monopolarization
245 started earlier in the eyes and brain than in the skin (Fig. S5A-D). However, the frequency of
246 monopolar mitotic cells with centriole loss reached over 50% in all these organs by 3 dpf,
247 revealing the general nature of the cellular defects in haploid larvae. These results
248 demonstrate that the haploidy-linked centriole loss observed in cultured mammalian cells
249 also occurs in haploid zebrafish larvae, causing severe mitotic dysregulation found to
250 contribute to organ growth retardation (Fig. 5H).

251

252 **Haploid larvae suffer retinal ciliopathy**

253 In addition to their role in forming mitotic spindles, centrioles are also required to form cilia,
254 and failure in this process causes a variety of ciliopathies (33-35). Therefore, we addressed
255 the possibility that the haploidy-linked centriole loss damages cilia-dependent processes.
256 Because retinal degeneration is a common ciliopathy condition (36, 37), we investigated
257 retinal organization in 5 dpf haploid and diploid larvae by immunostaining of zpr-1 and
258 acetylated-α-tubulin, which mark cone photoreceptors and cilia, respectively (34, 38). In
259 diploids, the zpr-1-positive photoreceptors aligned in the apical-most layer of the retina and

260 contained cilia at the outer retinal segment (Fig. 7A and B). On the other hand, in haploids,
261 the retinal layer was degenerated, with zpr-1-positive photoreceptors frequently mislocated
262 away from the apical region of the eye (Fig. 7A). A substantial proportion of apical-most
263 cells lacked acetylated-α-tubulin staining, indicating a severe impairment of ciliogenesis in
264 haploids (Fig. 7B). Therefore, the haploidy-linked centriole loss likely causes multifaceted
265 centriolar defects during development in haploid larvae through abnormal mitosis and
266 ciliogenesis.

267

Discussion

We investigated the cause of developmental defects in haploid zebrafish larvae at the cellular level. Our results revealed that haploid larvae suffer frequent cell death caused by mitotic defects associated with centrosome loss and irregular p53 upregulation. Mitigation of mitotic delay or p53 upregulation significantly improved organ growth in haploid larvae, suggesting that these defects in cell proliferation control are primary causes of the haploidy-linked organ growth retardation in zebrafish. Our findings also demonstrate a striking commonality of the cellular cause of apparently diverse developmental defects among haploid larvae in mammalian and non-mammalian vertebrates.

Poor organ growth is a common feature of haploid embryos in non-mammalian vertebrates. During several rounds of early cleavage, cell size in haploid embryos is equivalent to but gradually becomes smaller than that in diploids as embryonic development proceeds (22, 39). Therefore, haploid embryos have a higher demand for cell proliferation (i.e., need more cells) than diploids for achieving normal diploid-level organ size. Indeed, such compensatory cell number increase occurs in some cases, such as pronephric tubules and ducts in haploid newt larvae (40). However, this study found that haploid zebrafish larvae manifested frequent mitotic arrest across organs, likely blocking efficient cell proliferation during organogenesis. Moreover, resolution of mitotic arrest by SAC inactivation significantly improved organ growth in haploid larvae. Based on these results, we propose

289 that SAC-dependent mitotic arrest disables the compensatory cell number increase and
290 causes severe organ growth retardation in haploid larvae. A limitation of the experimental
291 approach using reversine is that SAC inactivation can resolve mitotic arrest and
292 accompanying defects but not chromosome missegregation caused by premature mitotic
293 exit without kinetochore-microtubule error correction (32), which may hinder the complete
294 restoration of mitotic fidelity and organ growth in this condition.

295

296 We found that the haploidy-linked centrosome loss commences around 1 dpf,
297 corresponding well to the timing of severe mitotic defects and organ growth defects
298 observed in haploid larvae. Most haploid larval cells with less than 2 centrosomes formed a
299 monopolar spindle, demonstrating that spindle bipolarization is inefficient upon centrosome
300 loss in these cells. In mammalian cultured cells and embryos, centrosome loss causes
301 chromosome missegregation and chronic mitotic delay resulting in gradual p53
302 accumulation that eventually blocks cell proliferation or viability (41-44). Therefore, it is
303 intriguing to speculate that the haploidy-linked p53 upregulation in zebrafish larvae stems
304 from severe centrosome loss. Interestingly, haploid mammalian cultured cells also suffer
305 centrosome loss and chronic p53 upregulation, limiting their proliferative capacity (1, 45).
306 Therefore, centrosome loss and p53 upregulation are common cellular defects associated
307 with the somatic haploid state in broad vertebrate species and are likely primary cellular
308 causes of organ growth retardation observed in haploid non-mammalian embryos.

309

Since the centriole serves as a basal body for ciliogenesis in differentiated postmitotic cells, the drastic centrosome loss potentially damages cilia-associated processes during the pharyngula period. Indeed, we found severe disorganization of the outer retinal layer with a drastic cilia loss in photoreceptors (Fig. 7). As we found progressive centrosome loss in all organs tested, ciliary malfunctioning would potentially take place in broader types of organs and contribute to pleiotropic defects of the haploid syndrome. Intriguingly, a previous scanning electron microscopy study has revealed a substantial loss of ciliated cells on the surface epithelia in haploid amphibian embryos (25). Therefore, further investigation of the causes and consequences of haploidy-linked ciliary defects would be an important subject in future studies.

In contrast to the later organogenetic stages, haploid embryos at 0.5 dpf possessed a normal number of the centrosomes, suggesting that early haploid embryos are free of severe centrosome loss. This result demonstrates that centrioles provided by the UV-irradiated sperms are functional to fully support centriole duplication during early developmental stages, excluding the possibility that centrosome loss in later haploid larvae is merely a side effect of sperm UV irradiation for gynogenesis. The reason for the lack of centrosome loss in early haploid embryos is currently unknown. Our previous study in human cultured cells revealed that the delay or absence of scheduled centriole duplication licensing causes the haploidy-linked centrosome loss (1). The structure and dynamics of the centrosomes in early fish embryos are remarkably different from those in somatic cells (46), and such an

early stage-specific mode of centrosomal control may enable the error-free centrosomal duplication even in the haploid state.

For further investigating the causality between centrosome loss and haploid developmental defects, it would be ideal to have an experimental condition that restores intact centrosomal control in haploid larvae. Previously, we found that artificial re-coupling of the DNA replication cycle and centrosome duplication cycle by delaying the progression of DNA replication resolved chronic centrosome loss and mitotic defects in human haploid cultured cells (2). Though we tried to restore centrosome loss by treating aphidicolin in haploid larvae, severe toxicity of the compound on haploid larvae after 1 dpf precluded us from testing its effect on centrosome control. Genetic manipulation of centrosome duplication control in haploid larvae may provide an excellent opportunity to directly investigate the causality of centrosome loss in the haploid syndrome in future studies.

Developmental incompetence of haploid larvae is likely a crucial evolutionary constraint of the diplontic life cycle (47). Though parent-specific genome imprinting would serve as the primary mechanism for blocking the development of haploid embryos in mammals, it has been unknown what precludes haploid development in non-mammalian species. Based on our results, we propose that the ploidy-centrosome link, as a broadly conserved mechanism, limits the developmental capacity of haploid embryos in non-mammalian vertebrates. It is

351 an intriguing future perspective to address how the ploidy-centrosome link is preserved or

352 modulated in invertebrate animal species, especially those with a haplodiplontic life cycle.

353

Material and Methods

Zebrafish strain and embryos

Wild-type zebrafish were obtained from National BioResource Project Zebrafish Core Institution (NZC, Japan) or a local aquarium shop (Homac, Japan). The *Tg(fli1:h2b-mCherry)/ncv31Tg* line (31) was provided by NZC. Transgenic animal experiments in this study were approved by the Committee on Genetic Recombination Experiment, Hokkaido University. Fish were maintained at 28.5°C under a 14 h light and 10 h dark cycle. To collect sperm for *in vitro* fertilization, whole testes from single male were dissected into 1 mL cold Hank's buffer (0.137 M NaCl, 5.4 mM KCl, 0.25 mM Na_2HPO_4, 0.44 mM KH_2PO_4, 1.3 mM $CaCl_2$, 1.0 mM $MgSO_4$ and 4.2 mM $NaHCO_3$). For sperm DNA inactivation, sperm solution was irradiated with 254 nm UV (LUV-6, AS ONE) at a distance of 30 cm for 1 min with gentle pipetting every 30 seconds (s). For insemination, we added 500 μL sperm solution to ~200 eggs extruded from females immobilized by anesthesia (A5040, Sigma-Aldrich; 0.08% ethyl 3-aminobenzoate methanesulfonate salt, pH 7.2). After 10 s, we added 500 mL Embryo medium (5 mM NaCl, 0.17 mM KCl, 0.33 mM $CaCl_2$, 0.33 mM $MgSO_4$ and 10^{-5}% Methylene Blue). After the chorion inflation, embryos were grown in Embryo medium at 28.5°C until use.

To inhibit pigmentation, we treated embryos with 0.03 g/L N-phenylthiourea (P7629, Sigma Aldrich) at 0.5 dpf. Dechorionation and deyolking were done manually in the cold

375 fish ringer's buffer without Ca^{2+} (55 mM NaCl, 1.8 mM KCl, 12.5 mM $NaHCO_3$, pH 7.2).
376 In the case of inducing p53 upregulation for checking the specificity of the anti-p53
377 antibody, diploid larvae were irradiated with 254 nm UV at a distance of 10 cm for 3 min at
378 66 hours post-fertilization (hpf). For SAC inactivation, larvae were treated with 5 μM
379 reversine (10004412, Cayman Chemical) from the timepoints described elsewhere.
380 Treatment with 0.5% DMSO was used as vehicle control for reversine treatment.

381

382 *Antibodies*

383 Antibodies were purchased from suppliers and used at the following dilutions: mouse
384 monoclonal anti-α-tubulin (1:800 for Immunofluorescence staining (IF); YOL1/34; EMD
385 Millipore); mouse monoclonal anti-β-tubulin (1:1000 for Immunoblotting (IB); 10G10;
386 Wako); mouse monoclonal anti-centrin (1:400 for IF; 20H5; Millipore); mouse monoclonal
387 anti-zpr-1 (1:400 for IF; ab17445; Abcam); rabbit monoclonal anti-active caspase-3 (1:500
388 for IF; C92-605; BD Pharmingen); rabbit polyclonal anti-p53 (1:1000 for IB; GTX128135;
389 Gene Tex); Alexa Fluor 488-conjugated rabbit monoclonal anti-acetylated-α-tubulin (1:200
390 for IF; D20G3; Cell Signaling Technology); Alexa Fluor 488-conjugated rabbit monoclonal
391 anti-phospho-histone H3 (pH3) (1:200 for IF and 1:50 for flow cytometry; D2C8; Cell
392 Signaling Technology); and fluorescence (Alexa Fluor 488, Alexa Fluor 594 or Alexa Fluor
393 647) or horseradish peroxidase-conjugated secondaries (1:100 for IF and 1:1000 for IB;
394 Abcam or Jackson ImmunoResearch Laboratories). Hoechst 33342 was purchased from
395 Dojinjo (1 mg/mL solution; H342) and used at 1:100.

396

397 *Flow cytometry*

398 For isolating whole-larval cells, ~ 10 deyolked embryos were suspended in cold trypsin
399 mixture (27250-018, Gibco; 0.25% trypsin in 0.14 M NaCl, 5 mM KCl, 5 mM glucose, 7
400 mM $NaHCO_3$, 0.7 mM EDTA buffer, pH 7.2) for ~15 min on ice with continuous pipetting.
401 For 2 dpf or older larvae, 8 mg/mL collagenase P (Roche) was added to the trypsin mixture
402 for thorough digestion. The isolated cells were collected by centrifugation at 1,300 rpm for
403 15 min at 4°C, fixed with 8% PFA in Dulbecco's phosphate-buffered saline (DPBS, Wako)
404 for 5 min at 25°C, permeabilized by adding the equal amount of 0.5% Triton X-100 in
405 DPBS supplemented with 100 mM glycine (DPBS-G), and collected by centrifugation as
406 above for removing the fixative. For DNA content and mitotic index analyses, cells were
407 stained with Hoechst 33342 and Alexa Fluor 488-conjugated anti-pH3, respectively, for 30
408 min at 25°C, washed once with DPBS, and analyzed using a JSAN desktop cell sorter (Bay
409 bioscience).

410

411 *Immunofluorescence staining*

412 For staining active caspase-3, pH3, zpr-1, or acetylated-α-tubulin, larvae were fixed with
413 4% PFA in DPBS for at least 2 h at 25°C, followed by partial digestion with cold trypsin
414 mixture for 3 min. For staining centrin and α-tubulin, larvae were fixed with 100%
415 methanol for 10 min at −20°C. Fixed larvae were manually deyolked in 0.1% Triton X-100

in DPBS and permeabilized with 0.5% Triton X-100 in DPBS overnight at 4°C, followed by treatment with BSA blocking buffer (150 mM NaCl, 10 mM Tris-HCl, pH 7.5, 5% BSA, and 0.1% Tween 20) for >30 min at 4°C. Larvae were subsequently incubated with primary antibodies for >24 h at 4°C and with secondary antibodies overnight at 4°C. Following each antibody incubation, larvae were washed three times with 0.1% Triton X-100 in DPBS. Stained larvae were mounted in Fluoromount (K024, Diagnostic BioSystems). For retinal imaging, eyes were manually isolated from whole-mount stained larvae for mounting on slides for imaging.

Microscopy

Immunostainings of active caspase-3, pH3, zpr-1, or acetylated-α-tubulin were observed on an A1Rsi microscope equipped with a 60× 1.4 NA Apochromatic oil immersion objective lens, a 100× 1.35 NA Plan-Apochromatic silicon oil immersion objective lens, an LU-N4S 405/488/561/640 laser unit, and an A1-DUG detector unit with a large-image acquisition tool of NIS-Elements (Nikon). For live imaging of histone H2B-mCherry-expressing larvae, the larvae were embedded in agarose gel (5805A, Takara) in E3 buffer supplemented with anesthesia and N-phenylthiourea and observed using a TE2000 microscope (Nikon) equipped with a Thermo Plate (TP-CHSQ-C, Tokai Hit; set at 30°C), a 60× 1.4 NA Plan-Apochromatic oil immersion objective lens (Nikon), a CSU-X1 confocal unit (Yokogawa), and iXon3 electron multiplier-charge-coupled device camera (Andor). Immunostaining of centrin and α-tubulin was observed on a C2si microscope equipped

with a 100× 1.49 NA Plan-Apochromatic oil immersion objective lens, an LU-N4 405/488/561/640 laser unit, and a C2-DU3 detector unit (Nikon).

Immunoblotting

Embryos were deyolked in cold-DPBS supplemented with cOmplete proteinase inhibitor cocktail (Roche, used at 2× concentration), extracted with RIPA buffer (50 mM Tris, 150 mM NaCl, 1% NP-40, 0.5% Sodium Deoxycholate and 0.1% SDS) supplemented with 2× cOmplete and centrifuged at 15,000 rpm for 15 min at 4°C to obtain the supernatant. Proteins separated by SDS-PAGE were transferred to Immun-Blot PVDF membrane (Bio-Rad). Membranes were blocked with 0.3% skim milk in TTBS (50 mM Tris, 138 mM NaCl, 2.7 mM KCl, and 0.1% Tween 20) and incubated with primary antibodies overnight at 4°C or for 1 h at 25°C and with secondary antibodies overnight at 4°C or 30 min at 25°C. Each step was followed by 3 washes with TTBS. For signal detection, the ezWestLumi plus ECL Substrate (ATTO) and a LuminoGraph II chemiluminescent imaging system (ATTO) were used. Signal quantification was performed using the Gels tool of ImageJ/Fiji software (NIH).

Measurement of larval body size

Larvae were anesthetized, mounted in 3% methylcellulose (M0387, Sigma), and observed under a BX51 transparent light microscope (Olympus) equipped with a 10× 0.25 NA

457 achromatic objective lens (Olympus) and a 20× 0.70 NA Plan-Apochromatic lens
458 (Olympus). We measured the body length, brain width, and lateral eye area of larvae using
459 the segmented line tool of ImageJ. Since haploid larvae were often three-dimensionally
460 curled or bent, we measured lengths of body axes viewed from lateral and dorsal sides and
461 used longer ones for statistical analyses. We realized that the severeness of the haploidy-
462 linked morphological defects tended to differ among larvae from different female parents.
463 Therefore, we used clutches of larvae obtained from the same female parents for
464 comparative analyses of the experimental conditions.

465

466 *Morpholino injection*

467 The morpholino used in this study were 5' -GCG CCA TTG CTT TGC AAG AAT TG- 3'
468 (p53 antisense) and 5' -GCa CCA TcG CTT gGC AAG cAT TG- 3' (4 base-mismatch p53
469 antisense) (48). One nL morpholino (dissolved in 0.2 M KCl with 0.05% phenol red at 3
470 mg/mL) was microinjected into haploid embryos at the 1 or 2 cell stage using FemtoJet and
471 InjectMan NI2 (Eppendorf).

472

473 *Statistical analysis*

474 Analyses for significant differences between the two groups were conducted using a two-
475 tailed Student's *t*-test in Excel (Microsoft). Multiple group analysis in Fig. 2B was
476 conducted using one-way ANOVA with Tukey post-hoc test in R software (The R

Foundation). Statistical significance was set at $p < 0.05$. p-values are indicated in figures or the corresponding figure legends.

Acknowledgment

We are grateful to Kentaro Kobayashi and other members of the Nikon Imaging Center at Hokkaido University for imaging technical support, Yoshimitsu Sagara, Kuniharu Ijiro, Hiroshi Hinou, and Shin-Ichiro Nishimura for microinjectors and microscopes, Mithilesh Mishra for kind supports, and the Open Facility, Global Facility Center, Creative Research Institution, Hokkaido University for the flow cytometer. This work was supported by JSPS KAKENHI (Grant Numbers JP19J12210, and JP21K20737 to K.Y., and JP19KK0181, JP19H05413, JP19H03219, JPJSBP120193801, and JP21K19244 to R.U.), the India Alliance Wellcome Trust/Department of Biotechnology Intermediate Fellowship IA/I/13/2/501042 to S.N., the Princess Takamatsu Cancer Research Fund, the Kato Memorial Bioscience Foundation, the Orange Foundation, the Smoking Research Foundation, Daiichi Sankyo Foundation of Life Science, and the Nakatani Foundation to R.U. The authors declare no competing financial interests.

Author Contributions

Conceptualization, K.Y., and R.U.; Methodology, K.Y., D.S., T.Me., T.Mi., T.K., S.N., and R.U.; Investigation, K.Y., and D.S; Formal Analysis, K.Y.; Resources, K.Y., D.S., T.Me., A.M., T.K., S.N., and R.U.; Writing – Original Draft, K.Y., and R.U.; Writing – Review & Editing, K.Y, T.Me., A.M., S.N., and R.U.; Funding Acquisition, K.Y., S.N., and R.U.

Figure legend

Figure 1. Morphological comparison between haploid and diploid larvae

(A) Transparent microscopy of haploid or diploid larvae at 3.5 dpf. Broken line: body axis (left panels), brain width (middle panels), or lateral eye contour (right panels). Arrowheads: curling or bending of body axis. Arrows: Edema. **(B)** Quantification of body axis length, brain width, or lateral eye area of haploid or diploid larvae in A. Box plots and beeswarm plots of at least 17 larvae (at least 34 eyes) from three independent experiments (**$p < 0.01$, two-tailed *t*-test).

Figure 2. Haploid zebrafish larvae suffer irregularly increased apoptosis

(A) Immunostaining of active caspase-3 and phospho-histone H3 (pH3) in whole-mount haploid or diploid larvae at 3 dpf. DNA was stained by DAPI. Z-projected images of confocal sections containing peripheral brain surface are shown. Broken lines indicate brain area. The arrowhead indicates clusters of apoptotic cells in the haploid larvae. **(B)** Classification of the level of apoptosis in haploid and diploid larvae. Seven haploid and 7 diploid larvae from two independent experiments were analyzed. All larvae observed in this experiment are shown in Fig. S2.

Figure 3. p53 upregulation limits organ growth in haploid larvae

(A, C) Immunoblotting of p53 in haploid, diploid, or UV-irradiated diploid larvae (A) or haploid larvae treated with control or p53 antisense morpholino (C) at 3 dpf. Arrows and open arrowheads indicate full-length and shorter p53 isoforms, respectively. β-tubulin was detected as a loading control. **(B, D)** Quantification of relative expression of p53 proteins in A (B) or C (D). Mean ± standard error (SE) of three independent experiments (*$p < 0.05$, **$p < 0.01$, one-way ANOVA with Tukey post-hoc test in B, and two-tailed t-test in D). **(E)** Immunostaining of active caspase-3 in whole-mount haploid control or p53 morphant at 3 dpf. DNA was stained by DAPI. Z-projected images of confocal sections containing peripheral brain surfaces are shown. Broken lines indicate brain area. The arrowhead indicates a cluster of apoptotic cells. **(F)** Classification of the level of apoptosis in haploid morphants. Six control morphants and 4 p53 morphants from two independent experiments were analyzed. All larvae observed in this experiment are shown in Fig. S3A. **(G)** Transparent microscopy of haploid control and p53 morphants at 3.5 dpf. Broken line: body axis (left panels), brain width (middle panels), and lateral eye contour (right panels). **(H)** Quantification of the body axis, brain width, and lateral eye area in G. Box plots and beeswarm plots of 29 larvae (58 eyes) from three independent experiments (**$p < 0.01$, two-tailed *t*-test).

Figure 4. Frequent mitotic delay and failures in haploid larvae

(A) Flow cytometric analysis of DNA content (Hoechst signal) and mitotic proportion (marked by anti-pH3) in isolated haploid or diploid larval cells at 1, 2, or 3 dpf. Magenta

boxes indicate the pH3-positive mitotic populations. **(B)** Quantification of mitotic index in A. Mean ± SE of at least three independent experiments (**$p < 0.01$, two-tailed *t*-test). **(C)** Live images of endothelial cells expressing histone H2B-mCherry in haploid or diploid larvae. Images were taken at a 7.5 min interval from 1.5 to 3 dpf. Asterisks indicate neighbor cells. **(D**, **E)** Distribution of mitotic length (time duration from NEBD to anaphase onset; D) or frequency of mitotic fates (E) in C. Data were sorted into separated graphs by mitotic fates (completion, mitotic death, or mitotic slippage) in E. At least 78 cells of 8 larvae from eight independent experiments were analyzed.

Figure 5. SAC inactivation mitigates abnormal mitotic patterns and organ growth defects in haploid larvae

(A) Live images of endothelial histone H2B-mCherry cells in haploid larvae treated with reversine approximately from 1.5 dpf. Images were taken at a 7.5 min interval from 1.5 to 3 dpf. **(B**, **C)** Distribution of mitotic length (B) or frequency of mitotic fates (C) in A. Data were sorted into separated graphs by mitotic fates (completion, mitotic death, or mitotic slippage) in C. At least 75 cells of 6 larvae from six independent experiments were analyzed. **(D)** Flow cytometric analysis of DNA content (Hoechst signal) and mitotic proportion (marked by anti-pH3) in the cells isolated at 3 dpf from haploid larvae treated with DMSO or reversine from 0.5 to 3 dpf. Magenta boxes indicate the pH3-positive mitotic populations. **(E)** Quantification of mitotic index in D. Mean ± SE of four independent experiments (*$p <$ 0.05, two-tailed *t*-test). **(F)** Immunostaining of pH3 in haploid 3-dpf larvae treated with

562 DMSO or reversine from 1.5 to 3 dpf. Z-projected images of confocal sections containing
563 peripheral brain surfaces are shown. Broken lines indicate brain area. **(G)** Transparent
564 microscopy of haploid 3.5-dpf larvae treated with DMSO or reversine from 1.5 to 3.5 dpf.
565 Broken line: body axis (left panels), brain width (middle panels), and lateral eye contour
566 (right panels). **(H)** Measurement of the body axis, brain width, and lateral eye area in G. Box
567 plots and beeswarm plots of 24 larvae (48 eyes) from three independent experiments (**$p <$
568 0.01, two-tailed *t*-test).

569

570 **Figure 6. Centrosome loss and spindle monopolarization in haploid larvae**

571 **(A)** Immunostaining of α-tubulin and centrin in haploid and diploid larvae at 0.5, 1, 2, and 3
572 dpf. Magenta boxes in left or middle panels indicate the enlarged regions of eyes (shown in
573 middle panels) or mitotic cells (shown in right panels), respectively. Insets in the right panels
574 show 3× enlarged images of centrioles. **(B**, **C)** Spindle polarity and centrin foci number in
575 mitotic cells in the whole-head region (including eyes, brain, skin epithelia, and olfactory
576 organ) at different developmental stages. Mean ± SE of at least 22 cells of at least 4 larvae
577 from two independent experiments (asterisks indicate statistically significant differences
578 from diploids at the corresponding time points; *$p < 0.05$, **$p < 0.01$, two-tailed *t*-test). Data
579 points taken from the eyes, the brain, or skin epithelia are also shown separately in Fig. S5.

580

581 **Figure 7. Retina disorganization in haploid larvae**

582 **(A**, **B)** Immunostaining of zpr-1 and acetylated-α-tubulin in an eye of haploid or diploid
583 larvae at 5 dpf. DNA was stained by DAPI. B shows an enlarged view of the outer retinal
584 segment at the region indicated by arrowheads in A. Representative data of at least 9 eyes
585 from two independent experiments.

586

Supplemental figure 1. Generation of haploid and diploid larvae

Experimental scheme of in vitro fertilization for generating haploid and diploid larvae (left) and flow cytometric DNA content analysis in Hoechst-stained larval cells (right; isolated from 3- or 5-dpf larvae). Representative data from two independent experiments are shown.

Supplemental figure 2. Visualization of apoptotic cells in haploid and diploid larvae

Immunostaining of active caspase-3 in whole-mount haploid and diploid larvae at 3 dpf. Z-projected images of confocal sections containing peripheral brain surface and inner brain area. We classified the severeness of apoptosis according to the degree of active caspase-3 staining. Arrowheads indicate clusters of apoptotic cells. Broken lines indicate brain area. All larvae analyzed in Fig. 2B are shown. The panel includes the larvae identical to those shown in Fig. 2A (marked by asterisks) to indicate the categories of their apoptotic levels.

Supplemental figure 3. Visualization of apoptotic cells in haploid control and p53 morphants

(A) Immunostaining of active caspase-3 in haploid control and p53 morphants at 3 dpf. Z-projected images of confocal sections containing peripheral brain surface and inner brain area. Arrowheads indicate clusters of apoptotic cells. Broken lines indicate brain area. All larvae analyzed in Fig. 3F are shown. The panel includes the larvae identical to those shown in Fig. 3E (marked by asterisks) to indicate the categories of their apoptotic levels. **(B)** Flow

607 cytometric DNA content analysis in Hoechst-stained larval cells isolated from haploid
608 control and p53 morphant at 3 dpf. Representative data from two independent experiments
609 are shown.

610

611 **Supplemental figure 4. Mitotic progression in haploid, diploid, or reveresine-treated**
612 **haploid larvae**

613 **(A-C)** Mitotic length plot against NEBD time point (dpf) in haploid or diploid larvae in Fig.
614 4C (A, B) or the reveresine-treated haploid larvae in Fig. 5A (C). At least 74 cells of 6 larvae
615 from six independent experiments were analyzed. **(D)** The frequency of mitotic fates of
616 haploid larval cells arrested at mitosis for > 60 min (shown as percentages in the total mitotic
617 events analyzed in A; 91 haploid larval cells of 8 larvae from 8 independent experiments).
618 Data were sorted by NEBD time point (dpf).

619

620 **Supplemental figure 5. Haploidy-linked centrosome loss in different organs**

621 **(A**, **B)** Immunostaining of centrin and α-tubulin in haploid and diploid larvae. Representative
622 data of skin (A) and brain (B) of haploid and diploid larvae at 0.5, 1, 2 and 3 dpf. Magenta
623 boxes in left or middle panels indicate the enlarged regions of each organ (shown in middle
624 panels) or mitotic cells (shown in right panels), respectively. Insets in the right panels show
625 3× enlarged images of centrioles. **(C**, **D)** Spindle polarity and centrin foci number in mitotic

626 cells in each organ at different developmental stages. At least 11 cells of 4 larvae from two

627 independent experiments were analyzed for each condition.

References

1. Yaguchi K*, et al.* (2018) Uncoordinated centrosome cycle underlies the instability of non-diploid somatic cells in mammals. *The Journal of cell biology* 217(7):2463-2483.
2. Yoshizawa K, Yaguchi K, & Uehara R (2020) Uncoupling of DNA Replication and Centrosome Duplication Cycles Is a Primary Cause of Haploid Instability in Mammalian Somatic Cells. *Frontiers in cell and developmental biology* 8:721.
3. Mable BK & Otto SP (1998) The evolution of life cycles with haploid and diploid phases. *BioEssays* 20(6):453-462.
4. Otto SP & Jarne P (2001) Haploids--Hapless or Happening? *Science* 292(5526):2441-2443.
5. Wutz A (2014) Haploid animal cells. *Development* 141(7):1423-1426.
6. Leeb M & Wutz A (2013) Haploid genomes illustrate epigenetic constraints and gene dosage effects in mammals. *Epigenetics & Chromatin* 6(1):41.
7. Tilghman SM (1999) The Sins of the Fathers and Mothers: Genomic Imprinting in Mammalian Development. *Cell* 96(2):185-193.
8. Kaufman MH (1978) Chromosome analysis of early postimplantation presumptive haploid parthenogenetic mouse embryos. *Journal of embryology and experimental morphology* 45:85-91.
9. Sagi I*, et al.* (2016) Derivation and differentiation of haploid human embryonic stem cells. *Nature* 532(7597):107-111.
10. Leeb M & Wutz A (2011) Derivation of haploid embryonic stem cells from mouse embryos. *Nature* 479(7371):131-134.
11. Varadaraj K (1993) Production of viable haploid Oreochromis mossambicus gynogens using UV-irradiated sperm. *Journal of Experimental Zoology* 267(4):460-467.
12. Fankhauser G & Griffiths RB (1939) Induction of Triploidy and Haploidy in the Newt, Triturus Viridescens, by Cold Treatment of Unsegmented Eggs. *Proceedings of the National Academy of Sciences of the United States of America* 25(5):233-238.
13. Nagy A, Rajki K, Horvárth L, & Csárnyi V (1978) Investigation on carp, Cyprinus carpio L. gynogenesis. *Journal of Fish Biology* 13(2):215-224.
14. Purdom CE (1969) Radiation-induced gynogenesis and androgenesis in fish. *Heredity* 24(3):431-444.
15. Oppermann K (1913) Die Entwicklung von Forelieneiern nach Befruchtung mit radium bestrahlten Samemfaden. . *Arch. Mikrosk. Anat.* 83(11):141-189.
16. Hertwig O (1911) Die Radiumkrankheit tierischer Keimzellen, Ein Beitrag zur experimentellen Zeugungs und Vererbungslehre. . *Arch. Mikrosk. Anat.* 77(11):97-164.
17. Dasgupta S & Matsumoto L (1972) The haploid syndrome in isogenic haploid frog embryos of Rana pipiens derived by nuclear transplantation. *Journal of Experimental Zoology* 180(3):413-419.
18. Uwa H (1965) Gynogenetic haploid embryos of the Medaka (Oryzias Latipes). *Embryologia* 9(1):40-48.

19. Subtelny S (1958) The development of haploid and homozygous diploid frog embryos obtained from transplantations of haploid nuclei. *Journal of Experimental Zoology* 139(2):263-305.
20. Streisinger G, Walker C, Dower N, Knauber D, & Singer F (1981) Production of clones of homozygous diploid zebra fish (Brachydanio rerio). *Nature* 291(5813):293-296.
21. Menon T & Nair S (2018) Transient window of resilience during early development minimizes teratogenic effects of heat in zebrafish embryos. *Developmental dynamics : an official publication of the American Association of Anatomists* 247(8):992-1004.
22. Menon T, Borbora AS, Kumar R, & Nair S (2020) Dynamic optima in cell sizes during early development enable normal gastrulation in zebrafish embryos. *Developmental biology* 468(1-2):26-40.
23. Hamilton L & Tuft PH (1972) The role of water-regulating mechanisms in the development of the haploid syndrome in Xenopus laevis. *Development* 28(2):449-462.
24. Ellinger MS (1979) Ontogeny of melanophore patterns in haploid and diploid embryos of the frog, Bombina orientalis. *Journal of Morphology* 162(1):77-91.
25. Ellinger MS & Murphy JA (1980) Cellular morphology in haploid amphibian embryos. *Journal of embryology and experimental morphology* 59:249-261.
26. Kroeger PT, Jr., *et al.* (2014) Production of haploid zebrafish embryos by in vitro fertilization. *Journal of visualized experiments : JoVE* (89).
27. Luo C & Li B (2003) Diploid-dependent regulation of gene expression: a genetic cause of abnormal development in fish haploid embryos. *Heredity* 90(5):405-409.
28. Yamashita M (2003) Apoptosis in zebrafish development. *Comparative Biochemistry and Physiology Part B: Biochemistry and Molecular Biology* 136(4):731-742.
29. Sugiyama M, *et al.* (2009) Illuminating cell-cycle progression in the developing zebrafish embryo. *Proceedings of the National Academy of Sciences* 106(49):20812-20817.
30. Li Z, Hu M, Ochocinska MJ, Joseph NM, & Easter SS, Jr. (2000) Modulation of cell proliferation in the embryonic retina of zebrafish (Danio rerio). *Developmental dynamics : an official publication of the American Association of Anatomists* 219(3):391-401.
31. Yokota Y, *et al.* (2015) Endothelial Ca 2+ oscillations reflect VEGFR signaling-regulated angiogenic capacity in vivo. *eLife* 4.
32. Santaguida S, Tighe A, D'Alise AM, Taylor SS, & Musacchio A (2010) Dissecting the role of MPS1 in chromosome biorientation and the spindle checkpoint through the small molecule inhibitor reversine. *Journal of Cell Biology* 190(1):73-87.
33. Tsujikawa M & Malicki J (2004) Intraflagellar transport genes are essential for differentiation and survival of vertebrate sensory neurons. *Neuron* 42(5):703-716.
34. Kramer-Zucker AG, *et al.* (2005) Cilia-driven fluid flow in the zebrafish pronephros, brain and Kupffer's vesicle is required for normal organogenesis. *Development* 132(8):1907-1921.

35. Delaval B, Covassin L, Lawson ND, & Doxsey S (2011) Centrin depletion causes cyst formation and other ciliopathy-related phenotypes in zebrafish. *Cell cycle (Georgetown, Tex.)* 10(22):3964-3972.
36. Bujakowska KM, Liu Q, & Pierce EA (2017) Photoreceptor Cilia and Retinal Ciliopathies. *Cold Spring Harbor perspectives in biology* 9(10).
37. Shi Y, Su Y, Lipschutz JH, & Lobo GP (2017) Zebrafish as models to study ciliopathies of the eye and kidney. *Clinical nephrology and research* 1(1):6-9.
38. Larison KD & Bremiller R (1990) Early onset of phenotype and cell patterning in the embryonic zebrafish retina. *Development* 109(3):567-576.
39. Gibeaux R, Miller K, Acker R, Kwon T, & Heald R (2018) Xenopus Hybrids Provide Insight Into Cell and Organism Size Control. *Frontiers in physiology* 9:1758.
40. Fankhauser G (1945) Maintenance of normal structure in heteroploid salamander larvae, through compensation of changes in cell size by adjustment of cell number and cell shape. *Journal of Experimental Zoology* 100(3):445-455.
41. Fong CS*, et al.* (2016) 53BP1 and USP28 mediate p53-dependent cell cycle arrest in response to centrosome loss and prolonged mitosis. *eLife* 5.
42. Lambrus BG*, et al.* (2016) A USP28-53BP1-p53-p21 signaling axis arrests growth after centrosome loss or prolonged mitosis. *The Journal of cell biology* 214(2):143-153.
43. Meitinger F*, et al.* (2016) 53BP1 and USP28 mediate p53 activation and G1 arrest after centrosome loss or extended mitotic duration. *The Journal of cell biology* 214(2):155-166.
44. Bazzi H & Anderson KV (2014) Acentriolar mitosis activates a p53-dependent apoptosis pathway in the mouse embryo. *Proceedings of the National Academy of Sciences of the United States of America* 111(15):E1491-1500.
45. Olbrich T*, et al.* (2017) A p53-dependent response limits the viability of mammalian haploid cells. *Proceedings of the National Academy of Sciences of the United States of America* 114(35):9367-9372.
46. Rathbun LI*, et al.* (2020) PLK1- and PLK4-Mediated Asymmetric Mitotic Centrosome Size and Positioning in the Early Zebrafish Embryo. *Current Biology* 30(22):4519-4527.e4513.
47. Sagi I & Benvenisty N (2017) Haploidy in Humans: An Evolutionary and Developmental Perspective. *Developmental Cell* 41(6):581-589.
48. Langheinrich U, Hennen E, Stott G, & Vacun G (2002) Zebrafish as a model organism for the identification and characterization of drugs and genes affecting p53 signaling. *Current biology : CB* 12(23):2023-2028.

Figure 1

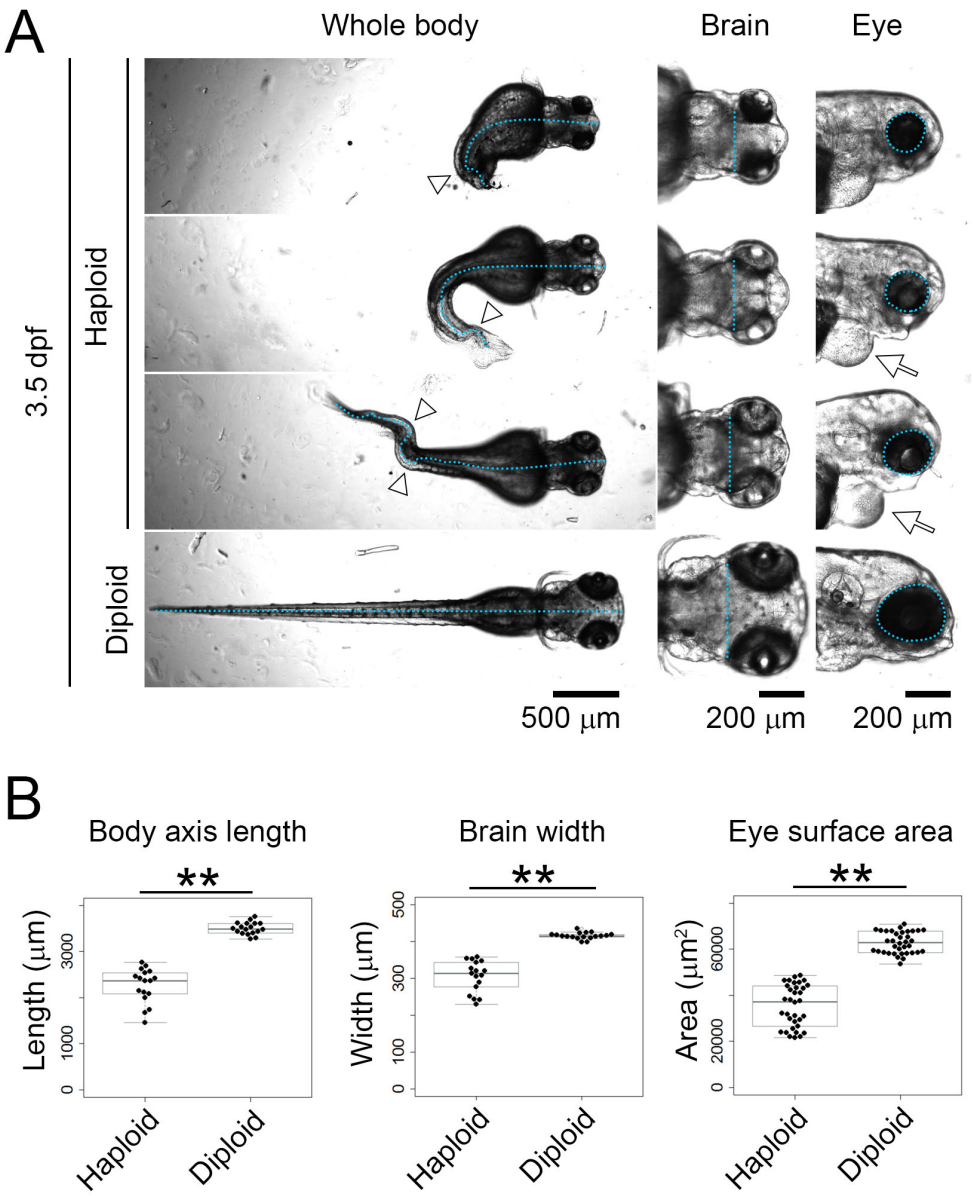

Figure 2

A

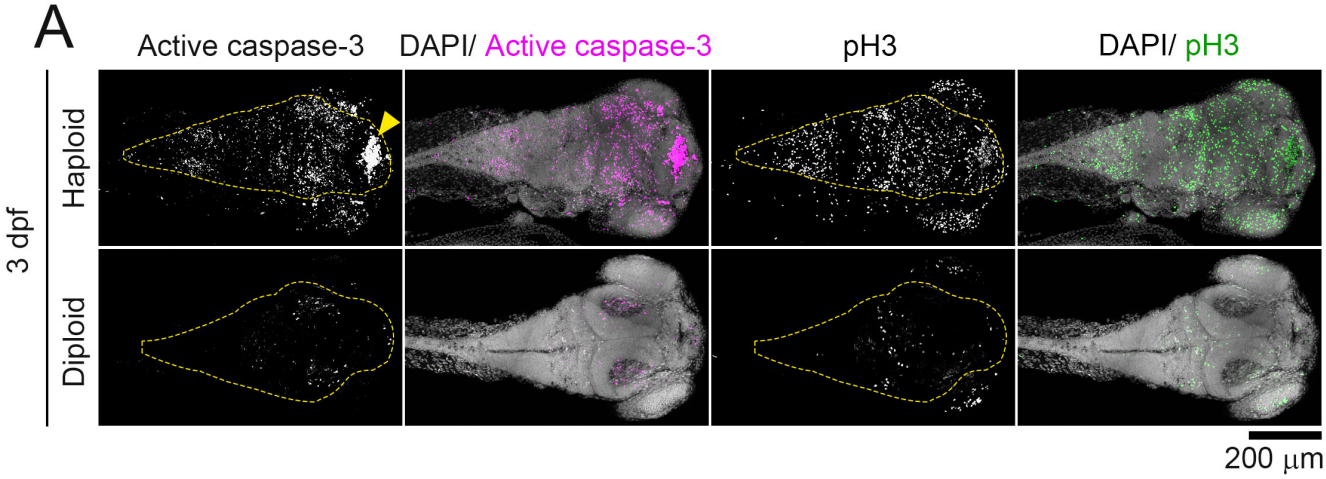

B

Apoptosis level	Haploid	Diploid
Scarce	None	2/7
Mild	2/7	5/7
Severe (w/ clusters)	5/7 (3 out of 5)	None (None)

Figure 3

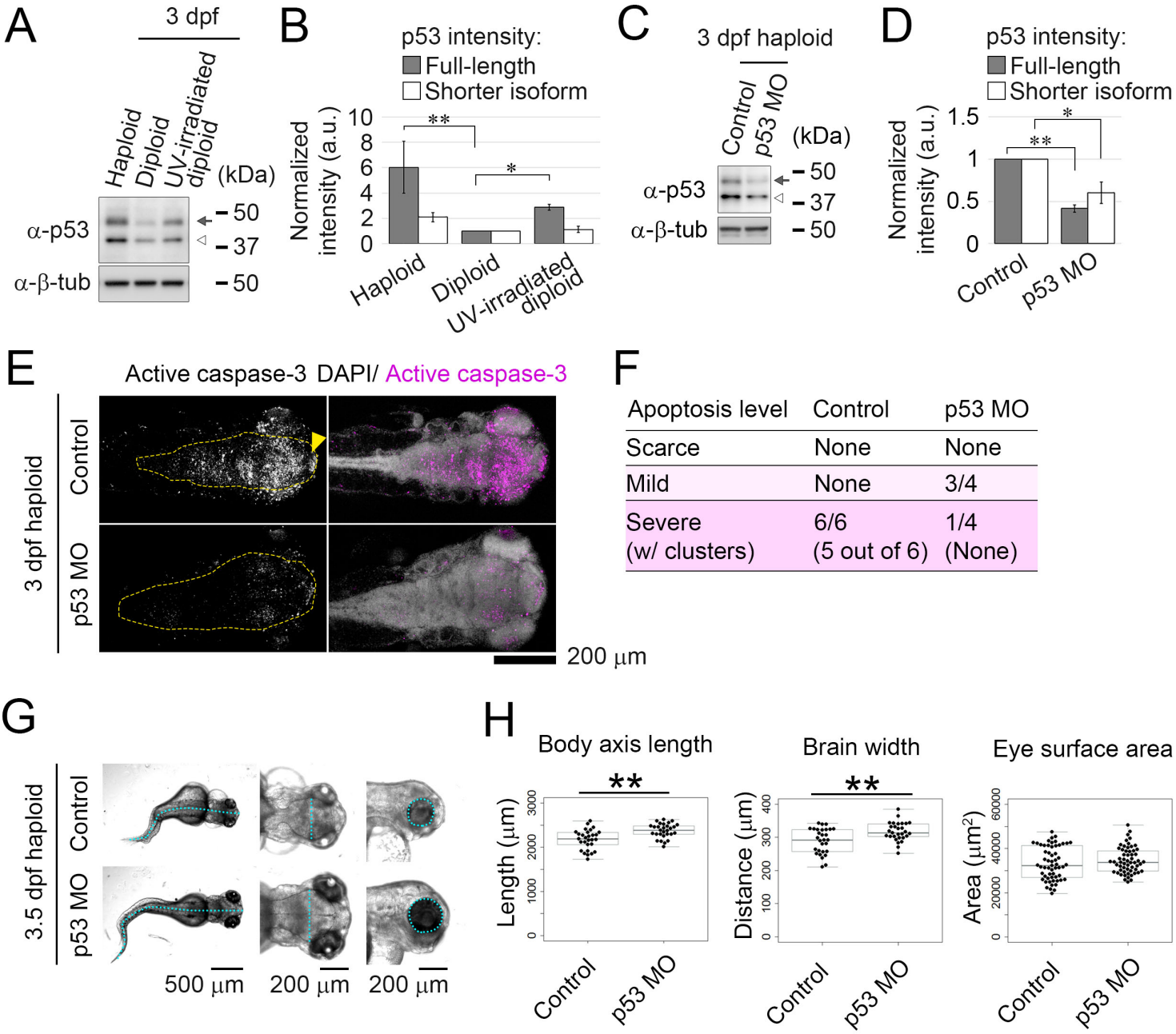

Figure 4

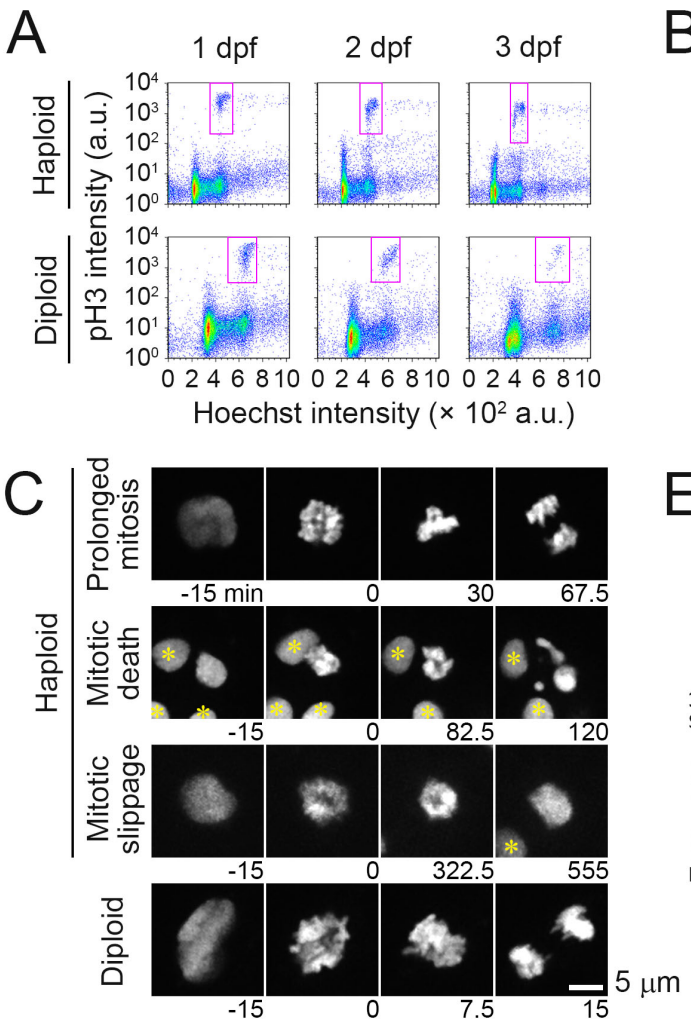

Figure 5

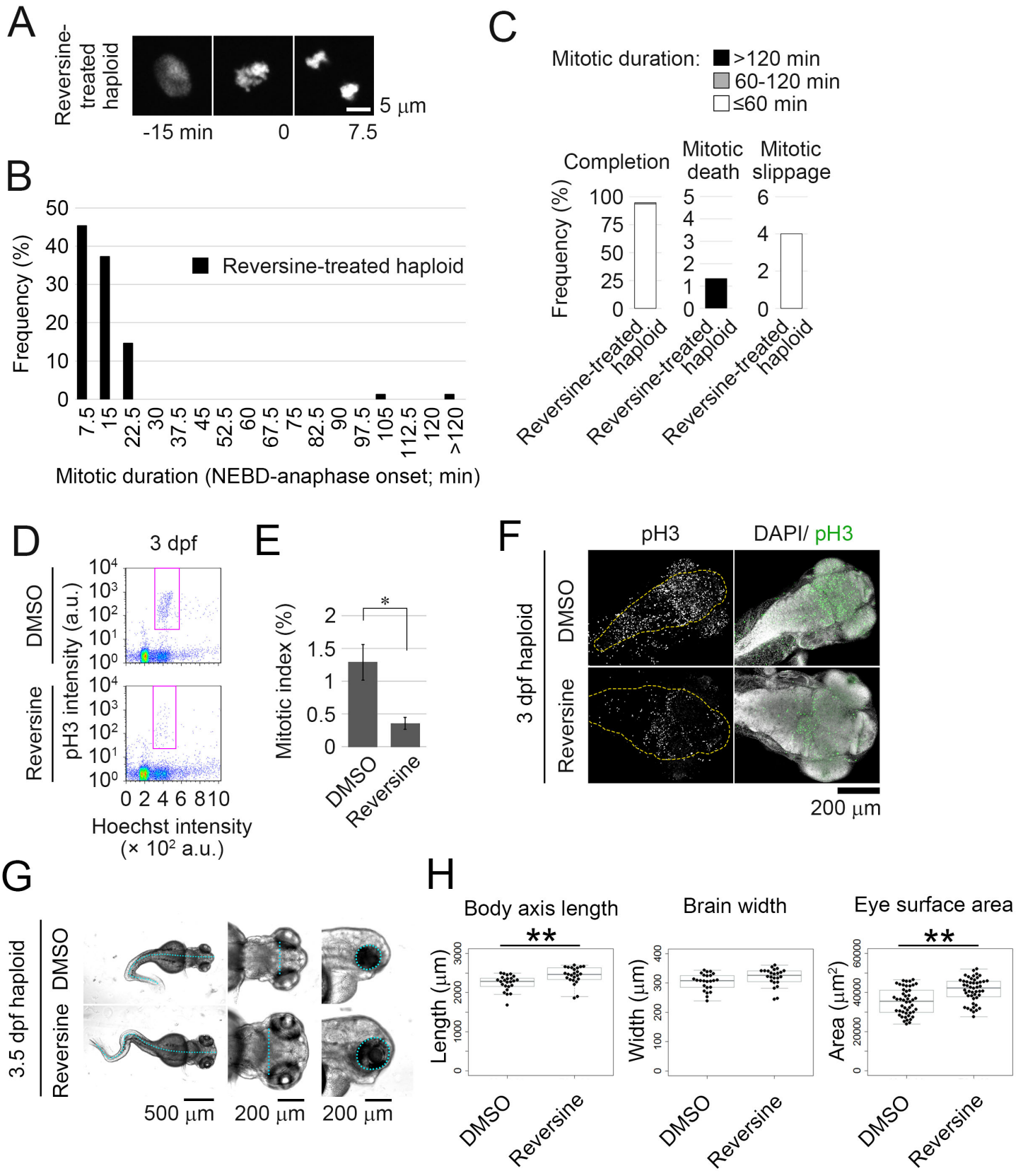

Figure 6

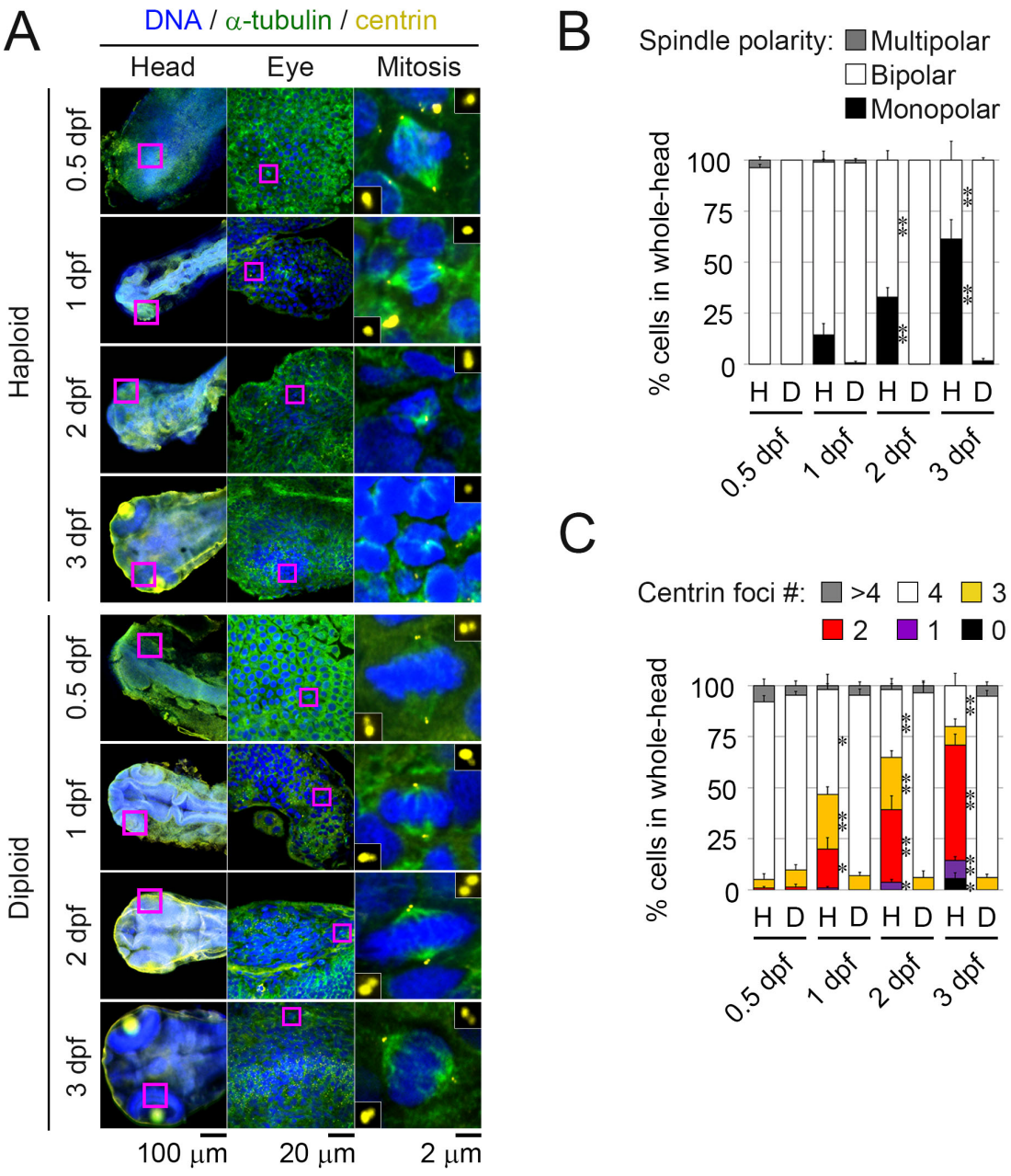

Figure 7

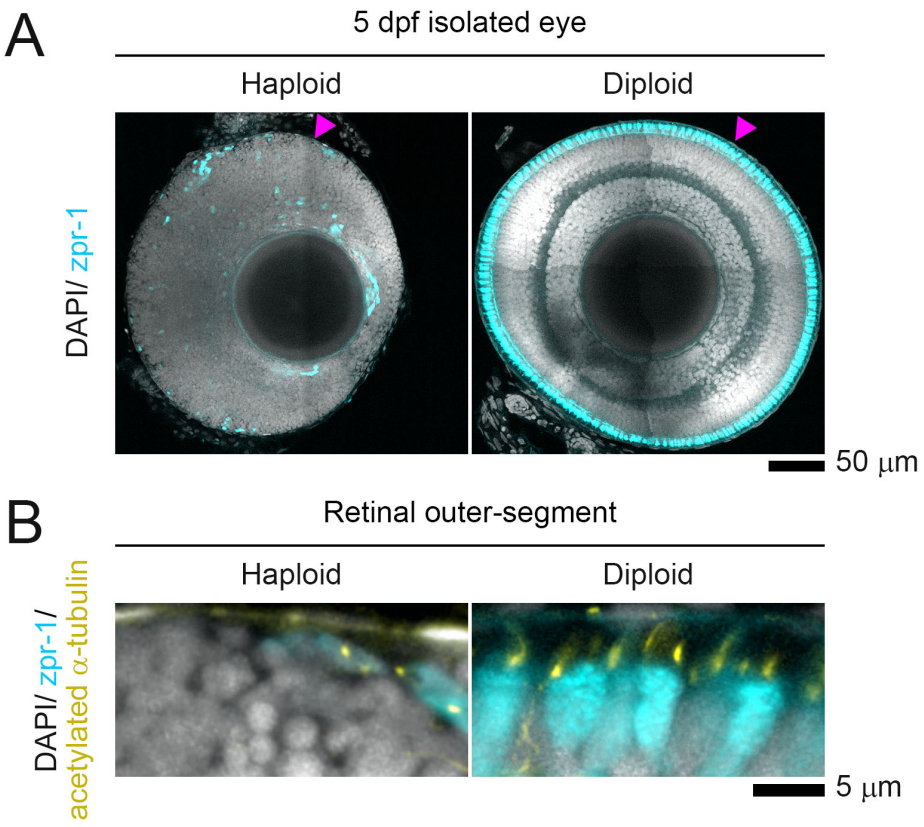

Supplemental figure 1

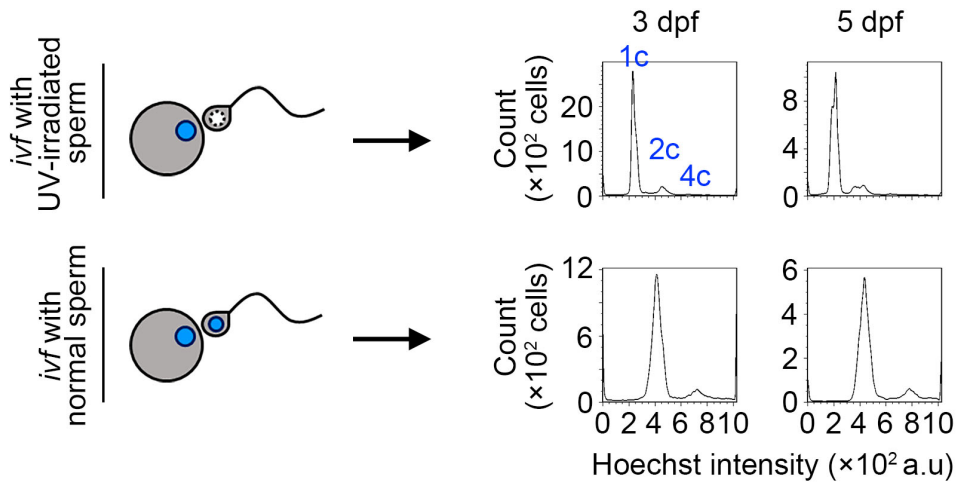

Supplemental figure 2

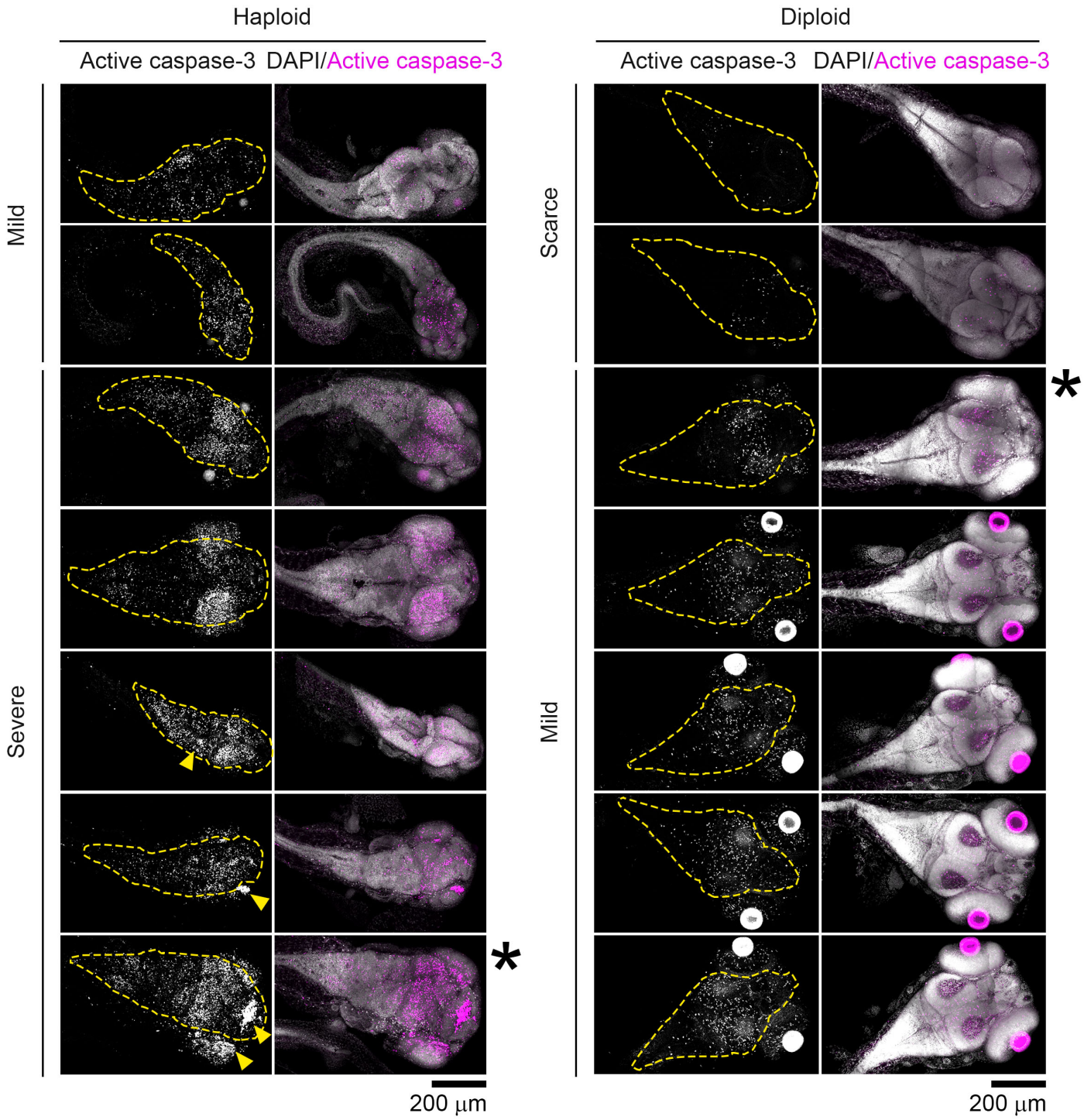

Supplemental figure 3

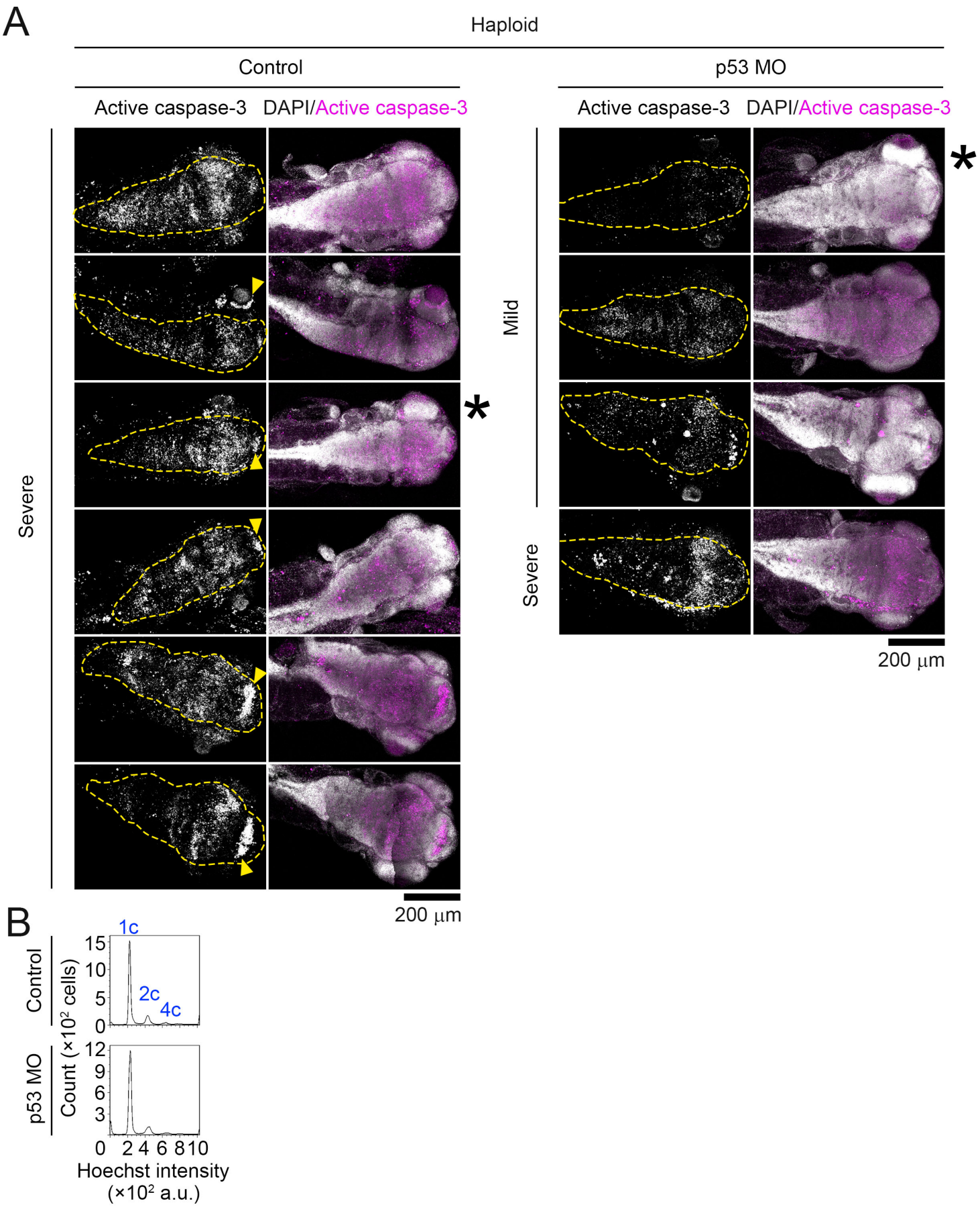

Supplemental figure 4

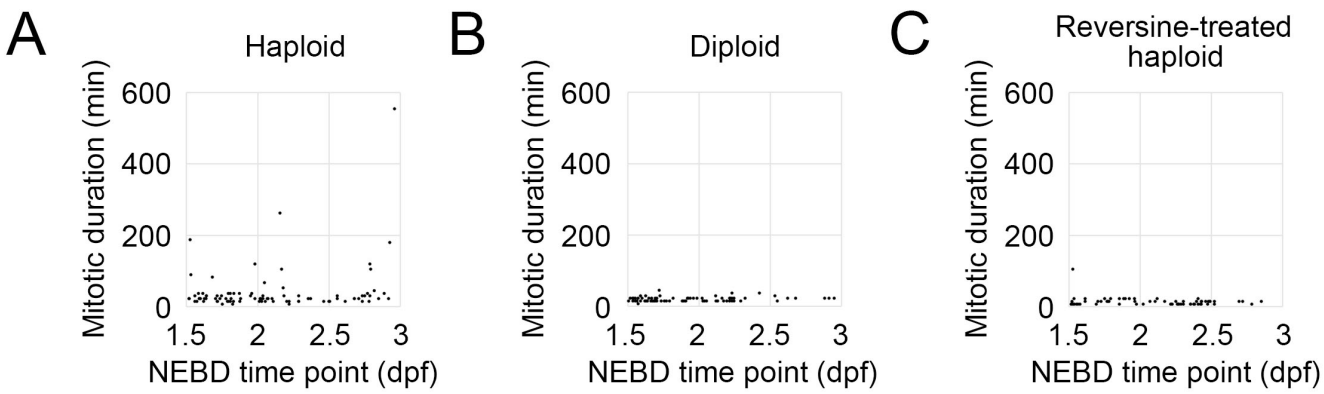

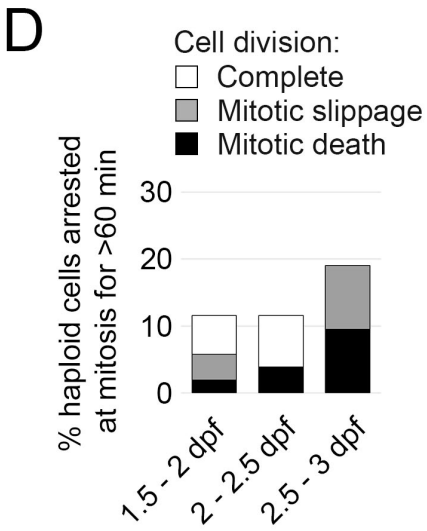

Supplemental figure 5